American Mineralogist, Volume 97, pages 329–340, 2012

MAS NMR measurements and ab initio calculations of the ^{29}Si chemical shifts in dumortierite and holtite

R. James Evans,[1] Colin A. Fyfe,[2] Lee A. Groat,[1,*] and Anita E. Lam[2]

[1]Department of Earth and Ocean Sciences, University of British Columbia, 6339 Stores Road, Vancouver, British Columbia V6T 1Z4, Canada
[2]Department of Chemistry, University of British Columbia, 2036 Main Mall, Vancouver, British Columbia V6T 1Z1, Canada

Abstract

Three samples from the dumortierite group of minerals were examined with magic angle spinning nuclear magnetic resonance spectroscopy (MAS NMR): a dumortierite [c. $(Al,\square)Al_6(BO_3)Si_3O_{13}(O,OH)_2$] consisting of dark blue euhedral crystals from Madagascar (D34); a fine-grained pale blue dumortierite from Island Copper mine, British Columbia, Canada (D12); and a creamy white holtite [c. $(Ta,Nb,\square,Al)Al_6(BO_3)(Si,Sb,As)_3O_{12}(O,OH,\square)_3$] from Szklary, Lower Silesia, Poland (WPH). Restricted Hartree-Fock ab initio electronic structure calculations were performed on model clusters with the goal of matching local environments of Si atoms to peaks in the ^{29}Si MAS NMR spectra. The spectrum of D34 showed five resolved peaks at –95.2, –92.6, –91.3, –89.1, and –86.5 ppm with deconvoluted peak area contributions of 57, 19, 7, 10, and 7%. Electronic structure calculations, cross-polarization MAS NMR measurements and relative intensities support assigning the peaks at –95.2 and –92.6 ppm to Si2 and Si1 sites, respectively, adjacent to fully occupied Al1 sites (i.e., Q^4 Si sites), and assigning the three remaining peaks to Si sites adjacent to vacant Al1 sites (i.e., Q^3 Si sites). Due to the complexity of the dumortierite structure, clusters composed of at least the first four shells of nearest neighbor atoms to the target Si atom are necessary to model Q^4 sites. The spectrum of D12 showed two main peaks at –93 and –95 ppm, with minor peaks below –90 ppm and above –100 ppm. The spectrum of WPH showed one broad peak at –93 ppm, likely containing both Si1 and Si2 signals, and two minor peaks below –90 ppm.

Single-crystal X-ray diffraction and structure refinement on D34 shows orthorhombic symmetry, *Pnma*, $Z = 4$, $a = 4.6882(1)$, $b = 11.7924(2)$, $c = 20.1856(3)$ Å, and $V = 1115.97(4)$ Å^3 with $R_1 = 0.0124$. Three distinct sub-sites of the face-sharing octahedral chain site Al1 were distinguished corresponding to sites with one vacancy above, with one vacancy below, and between two occupied sites; the vacancy-adjacent sites have the cation displaced to increase the Al^{3+}-Al^{3+} distance. Each sub-site is approximately ¼ occupied, suggesting that Al^{3+} cations in individual face-sharing octahedral chains are ordered as □-Al-Al-Al, although cations from chain to chain are disordered, preserving *Pnma* symmetry.

Powder X-ray diffraction measurements were performed on both D34 and D12. The unit cell of D12 was found to be $a = 4.7001(7)$, $b = 11.785(2)$, $c = 20.277(3)$ Å.

Keywords: Dumortierite, holtite, nuclear magnetic resonance, borosilicates, ab initio, single-crystal X-ray diffraction, powder X-ray diffraction, electron microprobe

Introduction

The dumortierite group of orthorhombic borosilicates comprises three isostructural minerals: dumortierite [c. $(Al,\square)Al_6(BO_3)Si_3O_{13}(O,OH)_2$], magnesiodumortierite [c. $(Mg,Ti,\square)Al_4(Al,Mg)_2(BO_3)Si_3O_{12}(OH,O)_3$], and holtite [c. $(Ta,Nb,\square,Al)Al_6(BO_3)(Si,Sb,As)_3O_{12}(O,OH,\square)_3$]. Dumortierite is by far the most widespread of the three minerals and is second only to tourmaline as the most abundant borosilicate in pegmatites and aluminous metamorphic and metasomatic rocks (Grew 1996). In contrast, magnesiodumortierite has only been found in ultrahigh-pressure rocks of the western Alps (Chopin et al. 1995; Ferraris et al. 1995), and holtite in pegmatites at Greenbushes, Western Australia, Voron'i Tundry, Kola Peninsula, Russia, and Szklary, Lower Silesia, Poland (e.g., Pryce 1971; Voloshin et al. 1977; Pieczka and Marszałek 1996; Groat et al. 2009; Pieczka et al. 2011). In addition to several distinctive structural features such as face-sharing Al octahedra and vacancies at both cation and anion sites, dumortierite, and holtite are distinctive among aluminosilicate minerals because they incorporate not only substantial amounts of the high-field strength lithophile elements Nb and Ta substituting for Al at octahedral sites, but also significant quantities of the chalcophile elements As and Sb substituting for Si at tetrahedral sites with a change of coordination (e.g., Groat et al. 2001).

We undertook this study to investigate whether magic angle spinning nuclear magnetic resonance (MAS NMR) could provide new information about substitutions and vacancies around Si and Al in the crystal structures of dumortierite and holtite, and whether ab initio electronic structure calculations can be used to identify the structural environments responsible for the peaks seen in the spectra.

* E-mail: lgroat@eos.ubc.ca

0003-004X/12/0203–329$05.00/DOI: http://dx.doi.org/10.2138/am.2012.3880

Crystallography of dumortierite and holtite

Golovastikov (1965) and Moore and Araki (1978) described the crystal structure of dumortierite as a design on the semi-regular planar net {6·4·3·4} in the *bc*-plane. The structure (Fig. 1) consists of a framework of two types of double chains of edge-sharing Al octahedra that run parallel to the *a*-axis: (1) cubic close-packed single chains containing the Al2 and Al3 sites that are joined to equivalent chains through edge-sharing, and (2) chains of face-sharing octahedral dimers containing the Al4 sites. The two types of double chains share corners and form small trigonal channels, containing BO_3 triangles, and large hexagonal channels, containing the Al1 sites in chains of face-sharing octahedra. The Al1 sites are surrounded by "pinwheels" of six SiO_4 tetrahedra, two Si1 and four Si2 sites, which connect the face-sharing chain to the double chain framework.

While the dumortierite structure is orthorhombic, the {6·4·3·4} net on which it is based has hexagonal symmetry. Dumortierite is thus strongly pseudo-hexagonal. The ratio *c/b* for dumortierite is typically close to 1.71, and in an idealized hexagonal structure would be equal to $\sqrt{3} \sim 1.732$. Dumortierite and holtite crystals are frequently twinned with domains related by 120° rotation about a threefold twin axis parallel to the *a*-axis.

The Al4 and Al2-Al3 double octahedral chains provide dumortierite with a rigid backbone parallel to the *a*-axis and large (~7 Å in diameter) hexagonal channels. This large space contained within an aluminate template may be one reason dumortierite and holtite can incorporate large, heavy atoms not normally observed in aluminosilicates; the Al and Si sites within the channel have room to shift, expand, and distort in response to large substituents. Hence, we are interested in the local structural environments present around the Si and Al1 sites, about which MAS NMR can provide information.

Most of the important crystal-chemical substitutions in the dumortierite group minerals occur in the hexagonal channels, for example (Ta^{5+}, Nb^{5+}) at Al1 and (As^{3+}, Sb^{3+}) at Si1 and Si2 in holtite (see below), (Mg^{2+}, Ti^{4+}) at Al1 in magnesiodumortierite, and significant vacancies at Al1 in all three minerals. The mean Al1-Al1 distance in dumortierite is ~2.35 Å, which is unusually short for face-sharing octahedra, and the Al1 site is on average 75% occupied (Moore and Araki 1978). The Al1 face-sharing chains are disordered, which results in an average chain length that can be adjusted to fit the repeat distance of the remaining octahedral framework in the structure (Moore and Araki 1978). Vacancies at the Al1 site are charge compensated by replacement of O atoms by OH somewhere in the structure. In dumortierite this is thought to occur primarily at the O2 and O7 positions (Moore and Araki 1978; Alexander et al. 1986; Werding and Schreyer 1990; Ferraris et al. 1995; Cempírek and Novák 2005; Fuchs et al. 2005), adjacent to vacant Al1 sites, pointing into the hexagonal channel. These OH positions are also bonded directly to Si sites and should be observable by ^{29}Si MAS NMR.

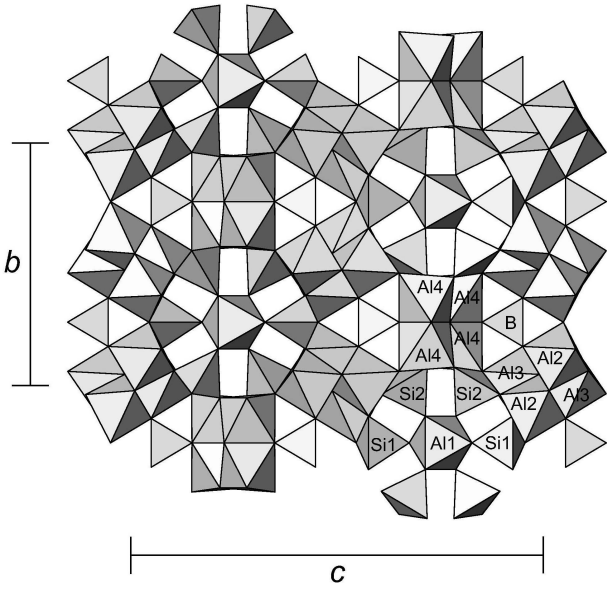

Figure 1. The structure of dumortierite observed along the *a*-axis.

Substitution of divalent cations for Al^{3+} in the Al4 or Al2-Al3 chains, as in magnesiodumortierite, is thought to be charge compensated by OH substitution at nearby O10, O9, or O1 sites (Ferraris et al. 1995; Farges et al. 2004). The presence of OH at the 4-coordinated O10 site is supported by bond valence analysis of the dumortierite structure, which shows O10 is underbonded, consistent with partial replacement of O by OH (Ferraris et al. 1995); OH is known to occupy the O10 position in magnesiodumortierite, which has a higher water content than dumortierite. The minerals ellenbergerite and phosphoellenbergerite, whose structures are hexagonal analogues of the dumortierite structure, are believed to contain OH at the 4-coordinated oxygen site equivalent to O10 in dumortierite (Raade et al. 1998; Brunet and Schaller 1996), as do several classes of synthetic materials with similar crystal structures (e.g., Marcos et al. 1993; Amorós et al. 1996), as well as the mineral holtedahlite, which has a different overall structure but features double octahedral chains similar to those that host the Al4 and O10 sites in dumortierite (Brunet and Schaller 1996). There is less evidence for OH at the O9 or O1 positions (Fuchs et al. 2005). Neither O10 or O9 are directly coordinated by silicon and so would not likely be observable by ^{29}Si MAS NMR.

Hoskins et al. (1989) determined that the crystal structure of holtite is closely related to that of dumortierite, but differs in several important respects, all of which lie within the hexagonal channels. Both SiO_4 tetrahedra are partially replaced by $Sb^{3+}O_3$ triangular pyramids with no evidence of preference of Sb for one of the Si sites, while Ta replaces Al at the Al1 position in an unrelated substitution. As a result, there are vacancies at the coordinating anion sites (O2 and O7) as well as at the Al1 site, unrelated to OH substitution. Relative to the Si positions, the Sb^{3+} sites are shifted about 0.5 Å closer to the Al1 position to accommodate the longer Sb^{3+}-anion bonds (average ~1.9 Å). When the Sb sites are occupied, the adjacent O2 (coordinating Si1) and O7 (coordinating Si2) positions are vacant (Fig. 2). With respect to OH, Hoskins et al. (1989) wrote that "…the (occupancy) factors obtained for O2 and O7…are in good agreement with the overall metal occupancy in Al1…For this reason there is not the need in holtite (as there is in dumortierite) for OH^- replacement of O^{2-} to provide a reduction in local charge to compensate for…a vacancy in Al1." Nonetheless, there have been reports (Voloshin

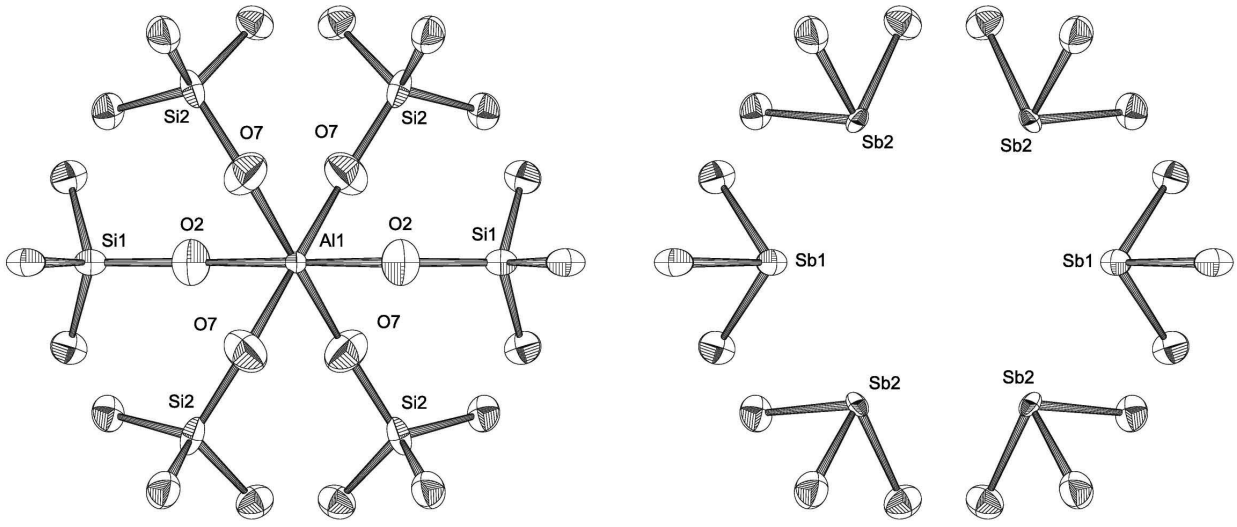

FIGURE 2. Disposition of SiO4 tetrahedra (**left**) and (Sb,As)O3 groups (**right**) and the coordinated central Al1 site in holtite (after Hoskins et al. 1989).

et al. 1977; Groat et al. 2009) of OH by infrared spectroscopy or single-crystal refinement. Groat et al. (2009) refined the crystal structures of holtite samples with different amounts of Sb (+As) and Ta (+Nb and Ti) and obtained the general formula $Al_{7-[5x+y+z]/3}(Ta,Nb)_x\square_{[2x+y+z]/3}BSi_{3-y}(Sb,As)_yO_{18-y-z}(OH)_z$, where x is the total number of pentavalent cations, y is the total amount of Sb + As, and $z \leq y$ is the total amount of OH. Holtite has not previously been examined by MAS NMR.

Previously, Choo and Kim (2003) used MAS NMR to study dumortierite samples from an Al-rich clay deposit in southeastern Korea. The ^{29}Si MAS NMR spectrum showed two peaks at –90.0 and –95.5 ppm, corresponding to the two Si sites in the crystal structure. The ^{27}Al MAS NMR spectrum showed only one asymmetrical peak near 0 ppm, suggesting no substitution of Al for Si. The ^{11}B MAS NMR spectrum showed one peak at 17.5 ppm, corresponding to B in triangular coordination.

EXPERIMENTAL METHODS

The number of dumortierite and holtite samples suitable for study by NMR was constrained by the need for 150 mg of clean material. Two samples of dumortierite and one of holtite were used in this study. Sample D34 is from Madagascar (source M. Pichavant). Sample D12 (Royal Ontario Museum sample M32888) is from the Island Copper mine in British Columbia, Canada. Holtite sample WPH (source A. Pieczka) is from the Szklary pegmatite in Poland, the same locality as sample H4 in Groat et al. (2009).

Dumortierite D34 consists of dark blue, euhedral crystals 1–3 mm across in a dominantly quartz matrix. Holtite WPH occurs as masses of creamy white crystals together with gray quartz and other minerals; its occurrence is described in Pieczka et al. (2011).

Sample D12 consists of very fine pale blue fibers (~5–10 µm in length) in a matrix of predominantly quartz and kyanite. The fibers were liberated from the matrix using a modified version of the method of Goreva et al. (2001) and Ma et al. (2002). Pieces of the sample were crushed to a grain size of 1–5 mm and dissolved in hot (100 °C) concentrated (48%) HF for several days, until no visible quartz remained, producing an insoluble residue with a color visually corresponding to the initial coloration of the dumortierite-rich parts of the sample. The mixture was dried overnight, after which the residue from the dissolution was treated with a 3:1 mixture of concentrated HF and HNO_3. The residue was then washed several times in a solution of 5% HNO_3 through agitation in an ultrasonic bath, followed by centrifuging, after which the liquid was pipetted away. The washing procedure was repeated several times with deionized H_2O in place of the acid. Finally the residue was dried on a hot plate at 150 °C. Upon drying, the sample produced a residue of visually homogeneous, fine-textured, flaky, blue-colored mats. The intensity of the coloration did not change during preparation and heating. Powder X-ray diffraction revealed the material to be dumortierite with minor amounts of aluminum fluoride hydrate and a rhombohedral SiO_2 phase as impurities (see below). The same procedure was used to remove quartz from holtite sample WPH. Solid-state ^{19}F MAS NMR spectra of these samples revealed no traces of fluorine incorporation whatsoever, even after very substantial numbers of scans.

The samples were first studied with a Philips XL30 scanning electron microscope equipped with an energy-dispersion X-ray spectrometer. Compositions of samples D34 and WPH (Table 1) were obtained with a fully automated CAMECA SX-50 microprobe, operating in the wavelength-dispersion mode with the following operating conditions: excitation voltage, 20 kV; beam current, 20 nA; peak count time, 20 s; background count time, 10 s; beam diameter, 10 µm. Data reduction was done with the "PAP" $\phi(\rho Z)$ method (Pouchou and Pichoir 1985). For the elements considered, the following standards and X-ray lines were used: kyanite, Al$K\alpha$, Si$K\alpha$; apatite, P$K\alpha$; rutile, Ti$K\alpha$; synthetic fayalite, Fe$K\alpha$; tennantite, As$K\alpha$; columbite, Nb$L\alpha$; tetrahedrite, Sb$L\alpha$; microlite, Ta$M\alpha$. Formulas were calculated on the basis of 18 (O + F + As + Sb) per formula unit and assuming 1 B atom per formula unit (apfu). Calculation of formulas based on anions plus As and Sb takes into account the vacancies created at the O2 and O7 sites with occupation of the Sb sites (see Groat et al. 2009).

Single-crystal X-ray diffraction measurements of two crystals from D34 were made at C-HORSE (the Centre for Higher Order Structure Elucidation, in the Department of Chemistry at UBC) using a Bruker X8 APEX II diffractometer with graphite monochromated Mo$K\alpha$ radiation. Data were collected and integrated using the Bruker SAINT software package. Additional details are given in Table 2.

Powder X-ray diffraction data were collected from samples D12 and D34 at C-HORSE using a Bruker D8 Advance diffractometer equipped with a diffracted-beam graphite monochromator and a Cu X-ray tube operated at 40 kV and 40 mA. Data were collected from 5 to 100 °2θ with a scanning step of 0.02 °2θ. After the original data were collected, a silicon powder standard having a cell parameter of 5.43011(5) Å was added to the samples and a second set of data was collected for the purpose of cell parameter refinement. The cell parameters were refined using the TOPAS 4.2 crystallographic software package of Bruker AXS and by using the starting parameters from the single-crystal X-ray refinement of D34.

NMR experiments

Solid-state NMR measurements were performed using a Bruker Avance 400 spectrometer operating at frequencies of 400.13, 376.55, 104.267, 79.494, and 128.39 MHz for ^{1}H, ^{19}F, ^{27}Al, ^{29}Si, and ^{11}B, respectively, using Bruker probes with either 7 mm or 4 mm MAS rotors. ^{29}Si chemical shifts were referenced to tetramethylsilane (TMS) with Q_8M_8 {the cubic octamer $Si_8O_{12}[OSi(CH_3)_3]_8$} as external

TABLE 1. Average electron microprobe compositions of dumortierite D34 and holtite WPH used in this study with standard devaitions

	D34 5 analyses		WPH 113 analyses	
	Average	Std. dev.	Average	Std. dev.
P_2O_5	0.02	0.02	0.29	0.16
Nb_2O_5	0.03	0.02	0.25	0.06
Ta_2O_5	0.01	0.01	12.57	0.98
SiO_2	29.33	0.17	19.79	0.52
TiO_2	0.45	0.06	0.00	0.01
B_2O_3	5.87	0.01	5.02	0.02
Al_2O_3	60.20	0.18	46.00	0.31
Sc_2O_3	0.01	0.01	0.20	0.03
Fe_2O_3	0.42	0.06	0.01	0.01
As_2O_3	0.00	0.00	3.03	0.59
Sb_2O_3	0.01	0.01	7.29	1.21
MgO	0.45	0.05	0.00	0.00
F	0.04	0.03	0.09	0.06
O=F	–0.02	0.01	–0.04	0.03
Total	96.84	0.09	94.50	0.39
P^{5+}	0.002	0.002	0.028	0.016
Nb^{5+}	0.001	0.001	0.013	0.003
Ta^{5+}	0.000	0.000	0.395	0.031
Si^{4+}	2.897	0.015	2.285	0.060
Ti^{4+}	0.034	0.005	0.000	0.001
B^{3+}	1.000	0.000	1.000	0.000
Al^{3+}	7.006	0.020	6.259	0.029
Sc^{3+}	0.001	0.000	0.020	0.035
Fe^{3+}	0.031	0.004	0.001	0.010
As^{3+}	0.000	0.000	0.213	0.041
Sb^{3+}	0.000	0.000	0.347	0.058
Mg^{+}	0.067	0.007	0.000	0.000
F^{-}	0.013	0.009	0.034	0.022
As + Sb	0.000	0.000	0.560	0.091
Nb + Ta	0.001	0.001	0.408	0.039
O	17.987	0.009	17.407	0.092

Notes: Sodium, K, Mn, and Bi were sought but not detected. Formulas were calculated on 18 (O+F+As+Sb) apfu and assuming 1 B apfu.

TABLE 2. Single-crystal X-ray collection and refinement information for dumortierite D34

a (Å)	4.6882(1)
b (Å)	11.7924(2)
c (Å)	20.1856(3)
V (Å^3)	1115.97(4)
Space group	*Pnma*
Z	4
Crystal size (mm)	~0.2 × 0.2 x 0.2
D_{calc} (g/cm^3)	3.404
Radiation	Mo*K*α
Monochromator	Graphite
Total F_o	15002
Unique F_o	1452
$F_o > 4\sigma F_o$	1401
R_{int}	0.0179
L.s. parameters	152
Range of *h*, *k*, *l*	$-6 \le h \le 6$, $-15 \le k \le 15$, $-24 \le l \le 26$
R_1 for $F_o > 4\sigma F_o$	0.0124
R_1 for all unique F_o	0.0133
wR_2	0.0355
a_w	0.0140
b_w	0.7192
GooF (=*S*)	1.165
$\Delta\rho_{max}$ (e Å^{-3})	0.264
$\Delta\rho_{min}$ (e Å^{-3})	–0.190

Note: $w = 1/[\sigma^2(F_o^2) + (a_wP)^2 + b_wP]$ where $P = [\mathrm{Max}(F_o^2,0) + 2F_c^2)]/3$.

secondary reference, ^{19}F to $CFCl_3$ with the ^{19}F resonance of octadecasil as external secondary reference and ^{27}Al shifts to 1 *M* aluminum nitrate aqueous solution as external reference. In some cases, further experimental details of individual NMR experiments are given in the figure captions.

Electronic structure calculations

Ab initio electronic structure calculations were performed on model clusters to support identification of the structural environments responsible for peaks seen in the ^{29}Si spectrum. All calculations were performed in the gas phase approximation using restricted Hartree-Fock (RHF) in Gaussian 09 (Frisch et al. 2009). Geometry optimization of the model clusters were performed using the 6-31G* basis set (Francl et al. 1982; Gordon 1980). NMR chemical shifts were calculated relative to TMS using the gauge-including atomic orbital method (GIAO) (Cheeseman et al. 1996; Wolinski et al. 1990) with the 6–311++g(2d,p) basis set (Frisch et al. 1984; Clark et al. 1983; McLean and Chandler 1980; Raghavachari et al. 1980). Similar methods of calculating NMR chemical shifts using model clusters have been used in the past (Casanovas et al. 2000; Xue and Kanzaki 2000; Tossell 2001; Kubicki and Toplis 2002; Kubicki and Heaney 2003; Casserly and Gleason 2005).

Preliminary calculations were first performed on several test systems for calibration: TMS $Si(CH_3)_4$, to obtain the reference shielding constant; a single aqueous silicon tetrahedron, $Si(OH)_4$, alone and with four hydrogen-bonded water molecules; an aqueous tetrahedral dimer $H_6Si_2O_7$, alone and with six hydrogen-bonded water molecules; and quartz, modeled by $(SiO_4)[Si(OH)_3]_4$. The quartz model cluster was based on the quartz structure of Ikuta et al. (2007), consisting of the first three shells of nearest neighbor atoms to the central Si site; in the initial optimization step, Si and O positions were frozen and only H positions were optimized. The entire structure was optimized in the other systems. All model clusters were electrically neutral. The test calculations were performed with the above basis-sets using both RHF as well the B3LYP density functional theory for comparison.

Results of the test calculations are given in Table 3, compared with experimental results from the literature. The calculated chemical shifts for the molecules $Si(OH)_4$ and $H_6Si_2O_7$ agree well with measured values, with better agreement for the RHF level of theory. The presence of hydrogen-bonded molecules simulating an aqueous environment makes little difference for $Si(OH)_4$, but improves agreement for the dimer. Chemical shifts for both $H_6Si_2O_7$ and $H_6Si_2O_7{\cdot}6H_2O$ fall within the expected range for sorosilicates. For the quartz model system, RHF gives –104.1 ppm and B3LYP, –117.4 ppm, compared with an experimental determination of –107.1 ppm. RHF again produces the better estimate. The quartz results suggest an expected error of ±3 ppm when using third-nearest neighbor neutral clusters to model extended crystal structures.

NMR shielding constants depend on the local environment of the subject nucleus, in this case ^{29}Si. In structures consisting of networks of corner-sharing tetrahedra, clusters consisting of the third to the fourth shell of atoms from the target Si nucleus have been found to produce realistic ^{29}Si chemical shifts (cf. Casanovas et al. 2000; Xue and Kanzaki 2000; Casserly and Gleason 2005), where a "shell" is taken as the set of near-neighbor atoms bonded to atoms of the previous shell. Dumortierite is a complex system with its silica tetrahedra embedded in networks of corner-, edge- and face-sharing octahedra, so larger model clusters may be necessary to accurately model chemical shifts.

Dumortierite model clusters were constructed based on the refined structure of D34 with Al1 modeled by a single site (see below), consisting of the first three shells of nearest neighbor atoms to the Si1 and Si2 sites, respectively. The third shell clusters consist of the central SiO_4 tetrahedron, first nearest neighbor cations and their coordinating oxygen atoms. Hydrogen atoms were added to the terminal oxygen atoms to make the cluster electrically neutral, for final stoichiometry $SiAl_8O_{35}H_{42}$, which we label $3Q^4$. In the geometry optimization step of the calculations the Si, Al, and O positions were frozen and only the H positions were optimized. The Si1 and Si2 $3Q^4$ clusters are shown in Figure 3.

Note that out to the third shell the local environments of the Si1 and Si2 sites are topologically the same, differing primarily in that the Si1 environment has a mirror plane symmetry, whereas the Si2 environment does not. In the fourth shell of atoms from the Si sites, topological differences between the Al2-Al3 and Al4 double octahedral chains appear and the two environments are no longer equivalent. This topological difference is most likely of lesser importance to the ^{29}Si shielding at the two silicon sites than the difference in local symmetry.

The $3Q^4$ clusters represent a structure with no cation vacancies, where each corner of the SiO_4 tetrahedron is bonded to another cation, equivalent to Q^4 Si sites in corner-sharing structures (cf. Moravetski et al. 1996; Tossell 2001). Tetrahedra where one corner is a terminal O atom or OH group not bonded to another cation in the crystal structure are called Q^3 Si sites. When the Al1 site is vacant, atoms at two O2 and four O7 sites are left under-bonded. It is thought that three (O2, O7) sites per Al1 vacancy are occupied by OH for charge balance (Moore and Araki 1978; Alexander et al. 1986), although the exact location of the structural H position is undetermined. Vacancies at Al1 will therefore lead to some fully bonded Q^4 SiO4 groups being replaced by Q^3 SiO_3OH groups and under-bonded Q^3 SiO_4 groups. The under-bonded O atoms in Q^3

TABLE 3. Test calculations of ^{29}Si shielding constants and chemical shifts relative to TMS (ppm)

Structure	RHF		B3LYP		Experiment
	CS*	δ†	CS	δ	δ
$Si(CH_3)_4$ (TMS)	385.7	0.0	327.9	0.0	0.0
$Si(OH)_4$	457.2	–71.5	396.7	–68.8	–71§, –72‖
$Si(OH)_4 \cdot 4H_2O$	457.4	–71.7	398.3	–70.4	
$H_6Si_2O_7$	462.5	–76.8	402.9	–75.0	–80§ (aqueous dimer),
	462.5	–76.8	403.0	–75.1	–72 to –84# (various sorosilicates)
$H_6Si_2O_7 \cdot 6H_2O$	464.8	–79.1	405.2	–77.3	
	464.3	–78.6	404.9	–77.0	
Quartz‡, modeled by $(SiO_4)[Si(OH)_3]_4$	489.8	–104.1	445.3	–117.4	–107.1**

Note: Model cluster structures optimized with basis 6–31 g*, chemical shifts calculated by GIAO with basis 6–311++g(2d,p).
* Chemical shift (ppm).
† Relative to TMS (ppm).
‡ Silicon and O positions based on structure from Ikuta et al. (2007) and frozen during structure optimization.
§ Kinrade and Swaddle (1988).
‖ Moravetski et al. (1996).
Hansen et al. (2003), Smith et al. (1983).
** Smith and Blackwell (1983).

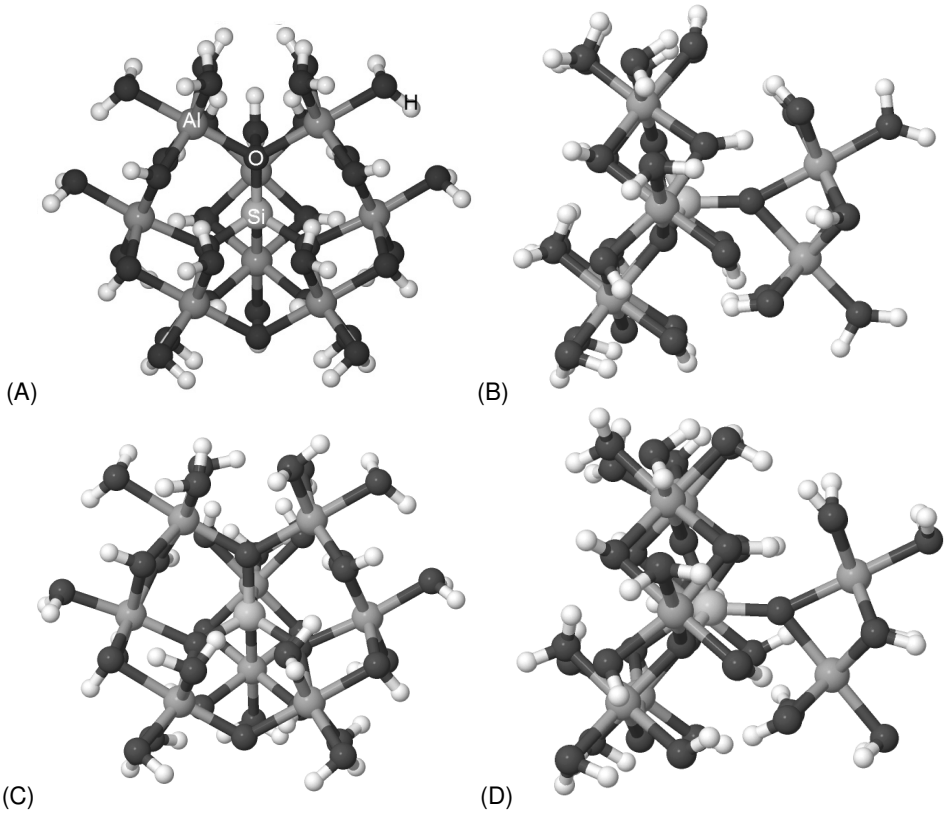

FIGURE 3. Model Q^4 clusters consisting of the third shell of atoms around the central Si atom, used in electronic structure calculations, with stoichiometry $SiAl_8O_{35}H_{42}$ ($3Q^4$). (**a** and **b**) Si1 $3Q^4$ cluster; (**c** and **d**) Si2 $3Q^4$ cluster.

SiO_4 groups are likely partially saturated through hydrogen bonding across the vacant Al1 site with OH groups in Q^3 SiO_3OH groups.

NMR parameters for Q^3 sites were calculated using model clusters based on the Q^4 clusters. The positions of all cations, O atoms, and coordinating H atoms were kept identical to the corresponding Q^4 clusters, with one Al atom removed from an Al1 site. Replacing one Al1 site in the $3Q^4$ cluster with three structural H on O2 and O7 sites leads to a model cluster with stoichiometry $SiAl_7O_{35}H_{45}$. The positions of the three structural H atoms were determined from separate calculations on a cluster with stoichiometry $Si_6Al_{14}O_{69}H_{72}$ (Fig. 4) that models the first three atomic shells around a vacant Al1 site, again derived from the D34 structure refinement with Al1 modeled by a single site. The Si, Al, and O positions were frozen and only H positions were optimized.

Two potential sets of positions for the structural H were investigated, each with all three H atoms on one face of the Al1 octahedron, pointing approximately toward the center of the empty site; in one case, the O-H bonds point up the *a*-axis, in the other, down the *a*-axis. Optimization of mixed configurations, i.e., with structural H on opposite faces of the Al1 octahedron, resulted in much higher relative energy clusters than all three H atoms on one face. Combined with two Al1 sites adjacent to each Si1 or Si2 site, this makes four possible configurations for a Q^3 Si site:

(1) Q^3 SiO_3OH with OH pointing down = Al1 vacancy below the Si site;
(2) Q^3 SiO_3OH with OH pointing up = Al1 vacancy above the Si site;
(3) Q^3 SiO_4 with OH pointing up = Al1 vacancy below the Si site;
(4) Q^3 SiO_4 with OH pointing down = Al1 vacancy above the Si site.

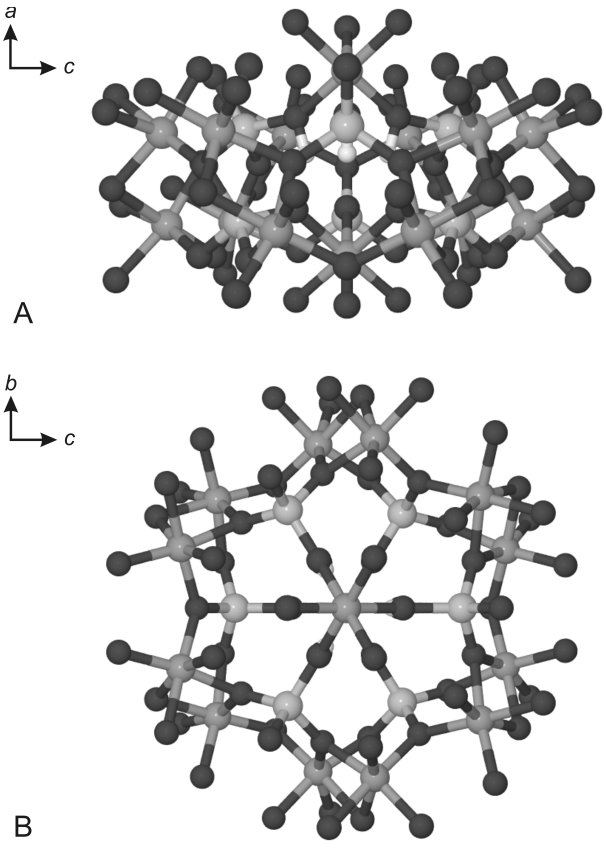

FIGURE 4. Model cluster to optimize OH positions and orientation within a vacant Al1 site, stoichiometry $Si_6Al_{14}O_{69}H_{72}$; charge-balancing H atoms are hidden for clarity.

The details of these configurations are show in Figures 5b–5e. Replacing the fully occupied Al1 sites in the $3Q^4$ cluster (Fig. 5a) with each of these four configurations in turn leads to four Q^3 model clusters that we label $3Q^3$-1 through $3Q^3$-4. Note that the vacant Al site makes these $SiAl_7O_{35}H_{45}$ clusters partially disconnected, with OH, OH_2, or OH_3 groups attaching to the main cluster through hydrogen bonding alone.

RESULTS

Electron microprobe

Average electron microprobe compositions of the dumortierite samples are given in Table 1. The totals are low, even if water is present. The fine-grained fibrous character of dumortierite and holtite is a possible cause of the low analytical totals. Grew et al. (2008) attributed low totals for analyses of finely porous material to contamination from epoxy filling the pores; similarly, epoxy could have filled the gaps between the very fine fibers of the dumortierite sample. In addition, we suspect that the data reduction routines are not able to completely correct for the effect of As, Sb, and Ta on Si and Al, elements not normally analyzed together.

The results show that sample D34 is almost end-member dumortierite; the main substituents are Mg (0.45 wt% MgO, or 0.07 Mg apfu), Ti (0.45 wt% TiO_2, or 0.03 Ti apfu), and Fe (0.42 wt% Fe_2O_3, or 0.03 Fe apfu). These are most likely to substitute for Al at the octahedral sites.

As expected, holtite sample WPH contains substantial amounts of As (3.03 wt% As_2O_3, or 0.21 As apfu), Sb (7.29 wt% Sb_2O_3, or 0.35 Sb apfu), and Ta (12.57 wt% Ta_2O_5, or 0.40 Ta apfu). Other substituents include P (0.29 wt% P_2O_5, or 0.03 P apfu), Sc (0.20 wt% Sc_2O_3, or 0.02 Sc apfu), and Nb (0.25 wt% Nb_2O_5 or 0.01 Nb apfu). No Ti was detected, which is unusual because Pieczka et al. (2011) and Groat et al. (2009) reported up to 3.82 wt% TiO_2 (0.30 Ti apfu) and 1.46 wt% TiO_2 (0.12 Ti apfu), respectively, in samples from this locality. In this sample Ta and Nb are expected to substitute at the Al1 site, and Sb and As at the Sb1 and Sb2 positions.

Microprobe analysis of D12 was unsuccessful due to the very fine-grained nature of the original sample and close association with kyanite, which appears identical to dumortierite under electron back scatter. Energy-dispersion spectra taken of both the whole rock and HF-digested powder show peaks for Ti and barely detectable Fe and P peaks; spectra of the powder also showed peaks from F (from the liberation process) and Ca (likely from the epoxy used to fix the powder to the stage). No significant heavy element or Mg peaks were observed.

Single-crystal X-ray diffraction

Refinement of the single-crystal X-ray diffraction data was performed using the SHELXTL crystallographic software package of Bruker AXS. Collection and refinement information for D34 is given in Table 2. Scattering factors for neutral atoms were used for the cations, and ionic factors for O^{2-}.

Initially all atoms were refined anistropically without any splitting of sites, leading to an R_1 of 0.0126. This is the model most generally used for dumortierite and holtite (cf. Moore and Araki 1978; Alexander et al. 1986; Groat et al. 2009). While most of the Al sites are relatively isotropic, with $U_{eq} = 0.0050(1)$, 0.0050(1), and 0.0069(1) Å^2 for Al2, Al3, and Al4, respectively, under this model the Al1 site is highly anisotropic, with $U_{11} = 0.0438(5)$, $U_{22} = 0.0062(3)$, $U_{33} = 0.0064(3)$, $U_{13} = 0.0022(3)$, and $U_{eq} = 0.0188(2)$ Å^2 (other off-diagonal terms are identically

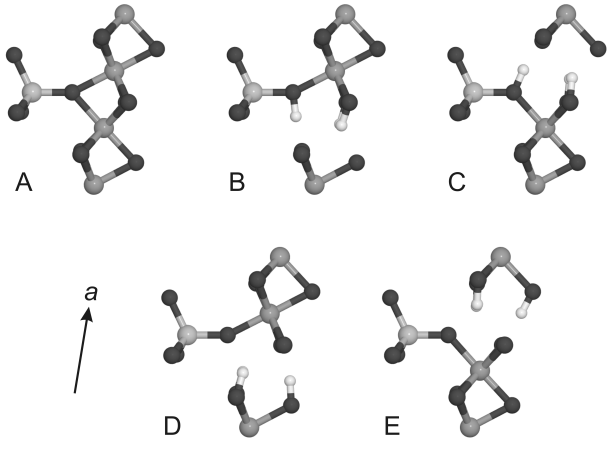

FIGURE 5. Schematics of different configurations possible for a Si site with one adjacent Al1 site vacant. The direction of the crystallographic *a*-axis is shown. (**A**) No adjacent Al1 sites vacant, a Q^4 SiO_4 site; (**B**) configuration 1 = Q^3 SiO_3OH with OH pointing down; (**C**) configuration 2 = Q^3 SiO_3OH with OH pointing up; (**D**) configuration 3 = Q^3 SiO_4 with OH pointing up; (**E**) configuration 4 = Q^3 SiO_4 with OH pointing down.

zero). The Al1 site has an occupancy of 0.756(2), which is typical for dumortierite. The high U_{11} factor indicates considerable positional displacement along the *a*-axis. When the Al1 site was reverted to isotropic and U_{iso} fixed at 0.0050 Å^2, two concentrations of electron density appeared below and above the Al1 site; these are labeled Al1a and Al1b, respectively. The occupancies of the three Al1 sites were then allowed to vary freely, with the sites restrained to have equal isotropic displacements. This lowered R_1 to 0.0124. The occupancies are 0.23(7), 0.28(5), and 0.24(9) for Al1, Al1a, and Al1b, respectively, and their shared U_{iso} = 0.0064(2) Å^2 is similar to the other Al sites. No other sites in the structure were significantly affected by the splitting of Al1. Atomic coordinates, displacement parameters, and bond lengths for the three-Al1-site model are given in Tables 4, 5, and 6, respectively. The earlier one-site model was used for refinement of the unit cells from powder X-ray diffraction and construction of model clusters for ab initio calculations.

The splitting of Al1 into three sites is likely due to vacancies in the hexagonal channels. Al1a is 0.24(5) Å below and Al1b 0.20(5) Å above the usual Al1 site. In the one-site model the Al1-Al1 distance across shared faces is $a/2$ = 2.3441 Å, an unusually short distance between trivalent cations. Cations in the face-sharing chain adjacent to a vacant Al1 site are likely to relax toward the vacancy due to Al^{3+}-Al^{3+} repulsion. Table 6 shows that the Al1a and Al1b sites each have a set of long (2.04–2.07 Å) and short (1.77–1.83 Å) Al-O bonds. The long bonds are likely adjacent to an occupied site, and the short bonds adjacent to a vacancy. The Al1a site is thus likely below another occupied site and above a vacancy, while the Al1b site is above an occupied site and below a vacancy. The usual Al1 site is either between two vacancies or two occupied sites. The occupancies of Al1, Al1a, and Al1b are all approximately equal to 0.25 within their respective errors, 1/3 of the total hexagonal channel octahedral site occupancy of 0.75, making the hexagonal channel octahedral site population approximately $(Al1a)_{0.25}(Al1)_{0.25}(Al1b)_{0.25}\square_{0.25}$. This suggests that the three sites occur in the hexagonal channel as trimers, with the Al^{3+} sites ordered in each channel as

$$\ldots - \square - Al1a - Al1 - Al1b - \square - Al1a - Al1 - Al1b - \square - \ldots$$

TABLE 4. Atomic coordinate parameters for dumortierite D34

	Multiplicity	*x*	*y*	*z*	Occupancy
Al1a	4	0.350(4)	3/4	0.2495(2)	0.28(5)
Al1	4	0.40(2)	3/4	0.2496(5)	0.23(7)
Al1b	4	0.443(7)	3/4	0.2508(3)	0.24(9)
Al2	8	0.55789(7)	0.61031(3)	0.47248(2)	0.988(2)
Al3	8	0.05981(7)	0.49095(3)	0.43096(2)	0.987(2)
Al4	8	0.05727(7)	0.35835(3)	0.28888(2)	0.996(2)
Si1	4	0.08701(9)	3/4	0.40557(2)	0.979(3)
Si2	8	0.58718(6)	0.52457(3)	0.32814(1)	0.982(2)
B	4	0.2255(4)	1/4	0.41611(8)	1
O1	4	0.3769(2)	3/4	0.45396(5)	1
O2	4	0.1492(3)	3/4	0.32597(6)	1
O3	8	0.8955(2)	0.63932(6)	0.42430(4)	1
O4	8	0.3997(2)	0.43611(6)	0.28257(4)	1
O5	8	0.3951(2)	0.55031(6)	0.39346(4)	1
O6	8	0.8808(2)	0.45421(6)	0.35013(4)	1
O7	8	0.6478(2)	0.63967(7)	0.28673(4)	1
O8	4	0.1621(2)	1/4	0.35067(5)	1
O9	8	0.2549(2)	0.35110(6)	0.44807(4)	1
O10	4	0.7611(2)	1/4	0.27214(5)	1
O11	8	0.7503(2)	0.46631(6)	0.48798(4)	1

Note: Occupancies of B and O sites were constrained equal to 1.

TABLE 5. Atomic displacement parameters for dumortierite D34 (× 10^{-4} Å^2)

	U_{11}	U_{22}	U_{33}	U_{23}	U_{13}	U_{12}	U_{eq}/U_{iso}
Al1							64(2)
Al1a							64(2)
Al1b							64(2)
Al2	50(2)	51(2)	49(2)	–1(1)	–3(1)	–2(1)	50(1)
Al3	49(2)	55(2)	47(2)	–1(1)	–1(1)	0(1)	50(1)
Al4	78(2)	66(2)	64(2)	11(1)	–8(1)	–1(1)	69(1)
Si1	43(2)	41(2)	82(2)	0	–2(1)	0	55(2)
Si2	49(2)	73(2)	48(2)	–11(1)	1(1)	1(1)	57(1)
B	59(7)	80(7)	65(7)	0	4(6)	0	68(3)
O1	60(5)	51(5)	89(5)	0	–13(4)	0	67(2)
O2	108(5)	146(6)	97(5)	0	23(4)	0	117(2)
O3	54(3)	51(3)	72(3)	2(3)	5(3)	–2(3)	59(2)
O4	57(3)	76(3)	56(3)	–10(3)	5(3)	–2(3)	63(2)
O5	59(3)	73(3)	50(3)	–7(3)	2(3)	–7(3)	61(2)
O6	66(4)	86(4)	57(3)	–16(3)	–5(3)	7(3)	70(2)
O7	111(4)	108(4)	127(4)	17(3)	14(3)	–16(3)	116(2)
O8	122(5)	56(5)	56(5)	0	–21(4)	0	78(2)
O9	86(4)	56(3)	61(3)	–5(3)	–17(3)	5(3)	68(2)
O10	68(5)	69(5)	105(5)	0	–4(4)	0	81(2)
O11	48(3)	56(3)	49(3)	2(3)	2(3)	–2(3)	51(2)

Note: Sites Al1, Al1a, and Al1b were constrained to have equal isotropic displacements.

TABLE 6. Bond distances for dumortierite D34 (Å)

Al1-O2^A	1.94(4)	Al1a-O2^A	2.07(1)	Al1b-O2^A	1.83(2)
Al1-O7	1.90(5)	Al1a-O7	2.05(1)	Al1b-O7	1.77(2)
Al1-O7^B	1.90(5)	Al1a-O7^B	2.05(1)	Al1b-O7^B	1.77(2)
Al1-O2	1.92(4)	Al1a-O2	1.81(1)	Al1b-O2	2.05(2)
Al1-O7^C	1.90(5)	Al1a-O7^C	1.77(1)	Al1b-O7^C	2.04(2)
Al1-O7^D	1.90(5)	Al1a-O7^D	1.77(1)	Al1b-O7^D	2.04(2)
<Al1-O>	1.91	<Al1a-O>	1.92	<Al1b-O>	1.92
Al2-O1	1.8904(6)	Al3-O3^F	1.9164(8)	Al4-O4	1.8532(8)
Al2-O3	1.8889(8)	Al3-O5^F	1.8798(8)	Al4-O4^C	1.8619(8)
Al2-O5	1.9045(8)	Al3-O6^F	1.8852(8)	Al4-O6^F	1.8684(8)
Al2-O9^E	1.8841(8)	Al3-O9	1.9172(8)	Al4-O8	1.8520(8)
Al2-O11^E	1.8817(8)	Al3-O11^F	1.8748(8)	Al4-O10^F	1.9170(9)
Al2-O11	1.9480(8)	Al3-O11^E	1.9298(8)	Al4-O10^C	2.0157(9)
<Al2-O>	1.8996	<Al3-O>	1.9005	<Al4-O>	1.8947
Si1-O1	1.674(1)	Si2-O4	1.6453(8)	B-O8	1.354(2)
Si1-O2	1.633(1)	Si2-O5	1.6254(8)	B-O9	1.363(1)
Si1-O3^F	1.6287(8)	Si2-O6	1.6673(8)	B-O9^H	1.363(1)
Si1-O3^G	1.6287(8)	Si2-O7	1.6192(8)	<B-O>	1.360
<Si1-O>	1.641	<Si2-O>	1.6393		

Note: A: x + 1/2, y, 1/2 – z; B: x, 3/2 – y, z; C: x – 1/2, y, 1/2 – z; D: x – 1/2, 3/2 – y, 1/2 – z; E: 1 – x, 1 – y, 1 – z; F: x – 1, y, z; G: x – 1, 3/2 – y, z; H: x, 1/2 – y, z.

moving up the *a*-axis. A significantly higher occupancy for the central Al1 site than the displaced Al1a or Al1b sites would suggest longer chains, whereas a much lower occupancy of the central site would suggest the predominance of dimers. Deviations of each site population from 0.25 indicates deviations from perfect ordering, as well as the difficulty in cleanly distinguishing the sites. While this ordering of Al1 sites occurs in individual hexagonal channels, the structure from channel to channel remains disordered, as there were no indications of a duplicated unit cell along the *a* direction. This arrangement is similar to that proposed by Moore and Araki (1978), while Alexander et al. (1986) suggested chains of 8–9 occupied sites per vacancy in the hexagonal channel. Ma et al. (2002) previously detected ordering between hexagonal channels in dumortierite fibers from rose quartz using high-resolution transmission electron microscopy, causing a doubling of the *b* and *c* unit-cell parameters

In the three site model, the minimum Al^{3+}-Al^{3+} distances in the hexagonal channel are now 2.54(5) Å between Al1-Al1b and

2.58(5) Å between Al1a-Al1; this is similar to the cross-face Al-Al distance in the Al4 chains of 2.5555(7) Å.

The presence of vacancies in the hexagonal channels also accounts for the large anisotropic displacement parameters for the O2 and O7 sites, which have U_{eq} = 0.0117(2) and 0.0116(2) Å^2, respectively, compared to 0.0059–0.0081 Å^2 at the other oxygen sites. Some O2 and O7 sites adjacent to vacant Al1 sites are expected to be occupied by OH^- for charge balance. A procedure similar to that described above for distinguishing the Al1a and Al1b sites did not identify any additional sites near O2 or O7.

A second crystal from D34 was collected and refined to R_1 = 0.0144 using the same model (with one-site model, R_1 = 0.0147) with similar results (not shown).

Powder X-ray diffraction

The powder X-ray diffraction patterns for D12 and D34 match well with the dumortierite patterns in the PDF-2 database and also with the calculated pattern from the single-crystal measurement of D34. Small peaks in the D12 pattern were found corresponding to an aluminum fluoride hydrate, which is likely a byproduct of the HF dissolution treatment, and an undissolved non-quartz SiO_2 phase.

The refined unit-cell parameters are given in Table 7. The powder unit-cell parameters for D34 are consistently slightly larger (~0.1%) than those determined from single-crystal measurements. The *c* parameter of D12, 20.277(3) Å, is significantly longer than those measured for D34 (20.18–20.20 Å). Similarly, the ratio *c*/*b*, given in the rightmost column of Table 6, is 1.7206(4) for D12 and very consistently 1.711–1.712 for D34 (both powder and single crystal). The elongated *c*-axis thus gives D12 a *c/b* ratio closer to the hexagonal ideal than D34.

NMR experiments

^{29}Si single pulse experiments were carried out with delays ranging between 1 and 120 s to ensure quantitative reliability for interpretation. A representative spectrum for D34 is shown in Figure 6. It was found that there were no differences in the spectral profiles over this very large range of delays indicating that the silicon (and proton) relaxation times are very short indeed. This is somewhat unusual for dense rigid materials and is thought to be due to the high concentration of protons establishing a spin temperature within the lattice and the presence of low levels of paramagnetic metal centers that act as efficient relaxation centers.

The D34 spectra show five resolved signals at approximately –95.2 (A), –92.6 (B), –91.3 (C), –89.1 (C), and –86.5 (E) ppm, although there is overlap. There is no indication of quartz impurity phase, in agreement with the powder XRD data, but this does not prove that none is present, as the spin lattice relaxation

TABLE 7. Comparing refined cell parameters of dumortierite samples D12 and D34

	a (Å)	*b* (Å)	*c* (Å)	*c/b*
D12 (powder)	4.7001(7)	11.785(2)	20.277(3)	1.7206(4)
D34 (powder)	4.6943(2)	11.8076(4)	20.2041(4)	1.7111(1)
D34 (single crystal)	4.6882(1)	11.7924(2)	20.1856(3)	1.7117(1)
	4.6875(2)	11.7953(5)	20.1886(8)	1.7116(1)

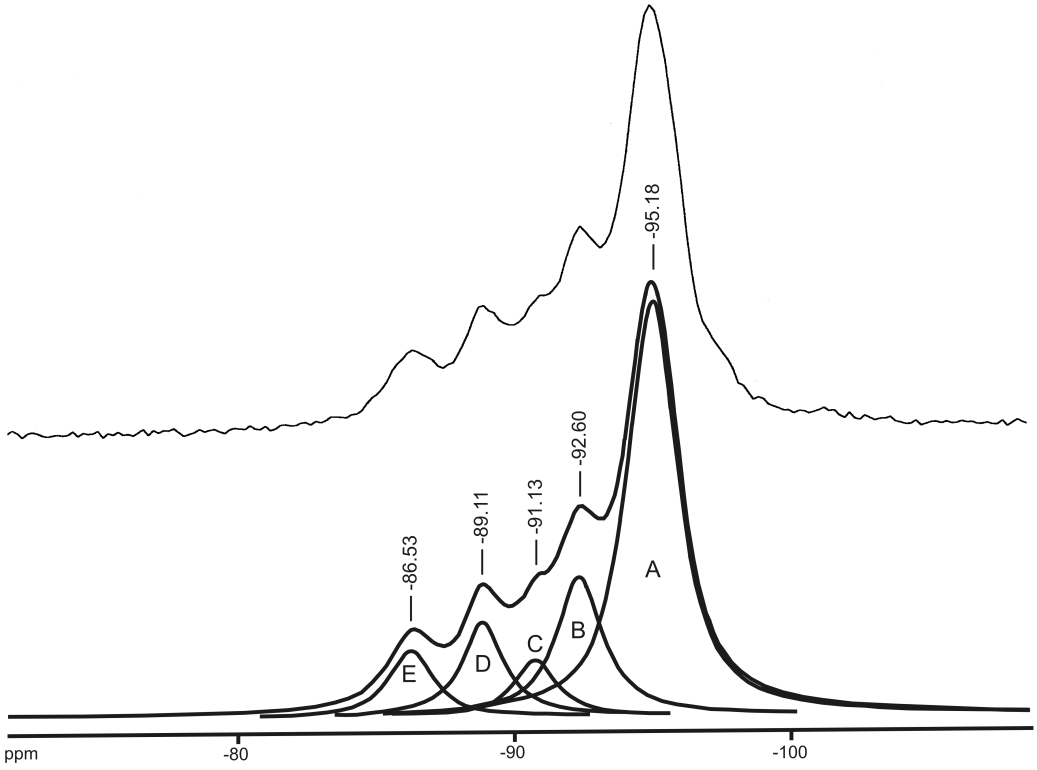

FIGURE 6. Experimental ^{29}Si single pulse MAS NMR spectrum of sample D34 with 30 s delay (**upper**). Deconvolution of this spectrum in terms of the five signals A–E as indicated, and their summation (**lower**).

time for quartz can be 1000 s or longer. It does, however, mean that it makes no contribution to the spectra. The chemical shifts are in the range previously reported by Choo and Kim (2003). The presence of several signals indicates that there are multiple silicon sites present, but the spectral overlap (probably due to line broadening from the disorder in the system) means that care must be taken not to over-interpret these data. There may even be lower intensity signals hidden in the center of the profile by the larger signals. The spectra can be deconvoluted, as shown in Figure 6, with the reliability of the resulting peak areas being highest for the outermost signals and those of higher intensities while the estimates of the inner peaks are much less accurate; estimates of the errors are ±10% for the outermost peaks; ±15% for the adjacent ones, and ±20% for the signal at the center of the spectrum. The results of such a deconvolution in terms of their percent contributions to the total area are: A, 57%; B, 19%; C, 7%; D, 10%; E, 7%. The chemical shift values of the two largest signals strongly suggest that they can be assigned to the two Q^4 silicon sites, Si2 and Si1, in the ideal framework where there has been no substitution. Although the relative intensities (~3:1) deviate from the expected 2:1 in the ideal structure where there has been no substitution of Al, there is ambiguity because of peak overlap and substitutions may affect the two sites differently. Further structural information can be obtained from a comparison between these Si spectra and those obtained from polarization transfer from the protons present in the system.

Two series of cross-polarization MAS NMR spectra were run, both with contact times between 0.1 and 10.0 ms, one with delay times of 1.0 s and the other 10.0 s. Both series gave identical results, as expected from the fast relaxation of the silicon spectra noted above. Representative spectra are shown in Figure 7. These provide complementary structural information to that from the single pulse experiments as they are not quantitative, but rather favor those nuclei closest to the source nuclei, in this case protons in the hydroxyl groups generated by Al1 vacancies. At very short contact times, the two lower field signals (D and E in Fig. 6) are greatly enhanced relative to the two high field signals compared to their intensities in the single pulse experiments and their maximum intensities are all reached after ~1 ms. Signal C (Fig. 6) also appears enhanced but there is more ambiguity here as this could be due to the higher intensities of D and E (Fig. 6). In contrast, the two higher field signals (A and B in Fig. 6) grow more slowly in intensity, never reaching the absolute intensities observed in the single pulse experiments. These data strongly suggest that the lower field signals are due to Q^3 silicons where OH substitution has occurred. This is also consistent with the change in chemical shift values from those of the two higher field signals. The general behavior is also very similar to that reported for the different Si sites in silica gel by Sindorf and Maciel (1980) and examined in detail by Klur et al. (2000) who showed that the C_P dynamics could be characterized as being in the "slow exchange regime." A similar situation was also found for layered silicates

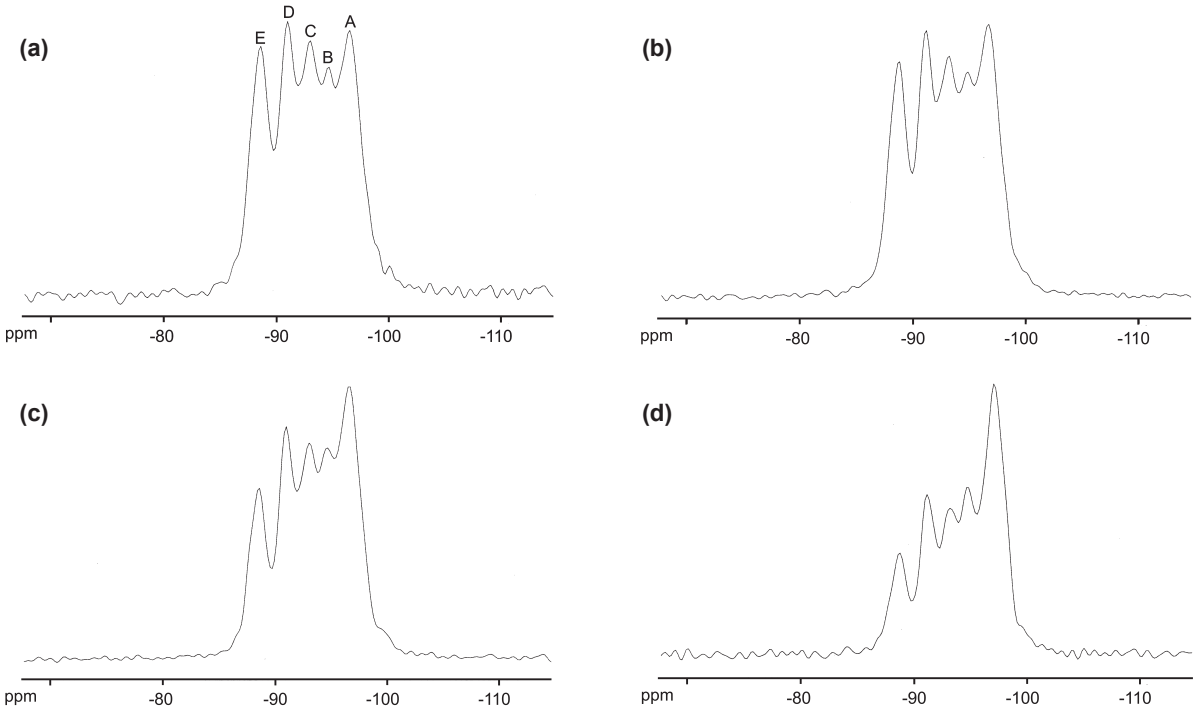

FIGURE 7. Cross-polarization ^{29}Si MAS NMR spectra of sample D34 with 1 s delay and contact times of (**a**) 0.2 ms, (**b**) 0.5 ms, (**c**) 1 ms, (**d**) 4 ms.

by Gardiennet et al. (2005) and appears to be characteristic of Q^3 Si-OH based polarization transfer from the hydroxyl protons, providing further support for this interpretation. It is not possible to provide more specific structural information on these sites from the present experiments, but it is worthwhile noting that the degree of substitution at the Al1 site is substantial, the three resonances accounting for approximately 22–27% of the total intensity of the quantitatively reliable single pulse silicon spectrum (Fig. 6).

The ^{29}Si MAS spectrum of sample D12 (Fig. 8a) shows several signals in addition to the most intense sharp one. The spectrum shows no evidence of major amounts of quartz or other impurities. As in the spectrum of D34, the main peak lies around –95 ppm, with a prominent shoulder around –93 ppm. Although less distinct than in D34, these two signals likely correspond to Q^4 Si2 and Si1 environments, respectively. The minor peaks to the left of the main peak below –90 ppm likely correspond to OH-adjacent Si sites. Cross-polarization experiments show an analogous behavior to those described above for sample D34, confirming the presence of OH groups. Two other minor peaks appear to the right of the main peak near –100 and –102 ppm (indicated by asterisks in Fig. 8a) which are thought to be due to the minor SiO_2 impurity observed in the D12 powder XRD pattern.

The ^{29}Si MAS spectrum of holtite sample WPH (Fig. 8b) shows one major peak and two very small ones. Compared to the D34 and D12 spectra, the main peak is shifted toward –93 ppm, and separate signals from Q^4 Si1 and Si2 are not observed. Broadening of the Q^4 peaks may in part be due to a mix of Al- and Ta-adjacent Si sites. The two very small peaks lie in the region corresponding to OH-adjacent Q^3 Si environments in sample D34, which supports the belief that OH is much less prominent in holtite. There are also two small peaks of unknown origin at higher field.

Fast-spinning ^{27}Al MAS spectra of both dumortierites (not shown) with very high S/N obtained using 14° pulse widths to ensure quantitative reliability showed only a single resonance at ~0 ppm with associated spinning sidebands, indicative of octahedral aluminum. Intensity in the range where tetrahedral aluminum would be expected was much less than 1%. This is in agreement with previous work. Electron microprobe analyses of sample D34 (Table 1), however, indicates a total 7.140 apfu octahedral cations excluding vacancies, in excess of the formula maximum of 7, and only 2.899 apfu tetrahedral (Si^{4+} + P^{5+}) cations vs. 3 tetrahedral sites per formula unit. Excluding tetrahedral Al^{3+}, this suggests either systematic errors with the microprobe analyses, or that smaller transition metal cations such as Ti^{4+} and Fe^{3+}, usually assumed to substitute for Al^{3+} at octahedral sites, are instead replacing some Si^{4+} at tetrahedral sites. With regard to the latter possibility, Farges et al. (2004) used XANES and EPR to determine that in dumortierite Ti^{4+} is mainly restricted to the Al1 hexagonal channel octahedral sites, whereas Fe is located mainly at Al2, Al3, and Al4 sites.

Fast spinning ^{11}B MAS spectra (not shown) are identical to that previously reported and shows a single resonance with considerable quadrupolar structure indicating a non-spherical local environment, consistent with trigonal boron as found by the diffraction experiments.

Electronic structure calculations

Calculated ^{29}Si shielding constants and chemical shifts for third-shell Q^4 and Q^3 model clusters are listed in Table 8. In general, the calculated chemical shifts are lower in magnitude (–80 to –90.4 ppm) than those observed in the spectrum (–86.5 to –95.2 ppm). Otherwise, the ordering of the chemical shifts for the model clusters agree well with the above interpretation of the spectra. The vacancy-adjacent Q^3 environments have significantly lower magnitude δ than the Q^4 environments. The calculated δ for Si2 environments is consistently higher in magnitude than δ for the corresponding Si1 environments. The Si2-Si1 splitting is 1.2 ppm for the Q^4 clusters, and an average of 1.3 ppm for the Q^3 clusters. This splitting is 2.6 ppm in the D34 spectrum and approximately 2 ppm in the D12 spectrum. All of these splittings, however, are smaller than the ±3 ppm error estimated from the quartz test calculations, so caution must be taken in their interpretation.

The chemical shifts calculated for different combinations of vacancy- and OH-placement relative to a Si Q3 site (illustrated schematically in Figs. 5b–5e) are grouped very closely together, within 1 ppm for configurations $3Q^3$-1, $3Q^3$-2, and $3Q^3$-3, so it is impossible to discern whether the multiple Q3 peaks in the experimental spectra are due to these different configurations. The $3Q^3$-4 configuration has a considerably lower magnitude δ than the rest in both Si1 and Si2 clusters; it is uncertain whether this is a genuine effect or an artifact of the model cluster geometry. In light of the single-crystal structure refinements, it is more plausible that the multiple Q3 peaks in the spectra are due to the split Al1 site, which was not taken into account in these calculations.

The low magnitude of the calculated chemical shifts is likely due to the complexity of the dumortierite structure and the size of the model clusters. In Table 3, we see that gas-phase RHF calculated chemical shifts agree very well with experimental values for the aqueous molecules $Si(OH)_4$ and $H_6Si_2O_7$, within 1 ppm for both clusters when neighboring hydrogen bonded waters are included. Agreement is less good for the third shell quartz model, but still within 3 ppm. In quartz, the corner of each SiO_4 tetrahedron is shared with only one other tetrahedral site. In dumortierite, each corner of the SiO_4 tetrahedra is shared with two AlO_6 octahedra in a more complicated structure, and the agreement of δ calculated with third shell Q^4 model clusters with experiment is only within about 6 ppm. The greater the connectivity of the ^{29}Si target nucleus and the more complex the surrounding structure, the poorer the approximation the relatively small third shell cluster is. Improving the accuracy of the chemical shift calculations would require additional shells of atoms around the target ^{29}Si. A fourth shell cluster modeling the Si1/Si2 sites would be terminated in highly under-bonded Al^{3+}, Si^{4+}, and B^{3+} cations; such highly charged clusters lead to unstable calculations and inconsistent results. The most reliable next level approximation would involve a fifth shell cluster, containing the target Si site's fully coordinated nearest and next-nearest neighbor cation sites, plus many additional H^+ to achieve a neutral cluster. This would involve model clusters of over 200 atoms and be much more computationally intensive.

Even without electronic structure calculations to determine exact Si environments corresponding to each peak, ^{29}Si MAS

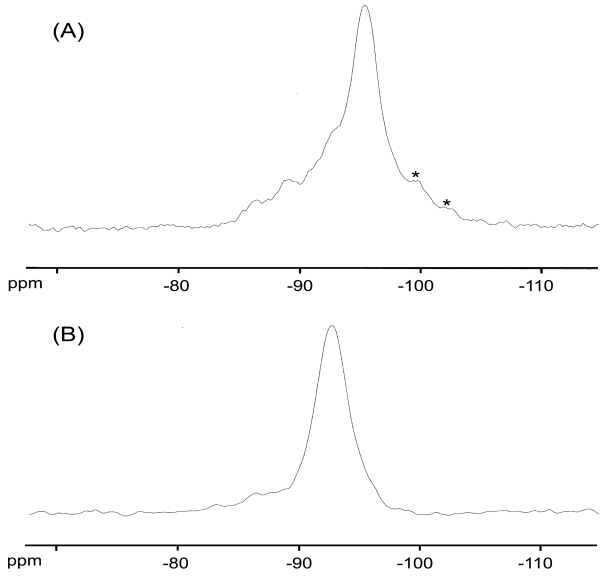

Figure 8. Single pulse ^{29}Si MAS NMR spectra of sample (**a**) D12 and (**b**) WPH with 30 s delay. * See text.

Table. 8. Calculated ^{29}Si shielding constants and chemical shifts relative to TMS (ppm) in dumortierite

Site	Si1		Si2	
Local environment	CS	δ	CS	δ
$3Q^4$	474.9	–89.2	476.1	–90.4
$3Q^3$-1	469.3	–83.6	470.2	–84.5
$3Q^3$-2	469.5	–83.8	470.0	–84.3
$3Q^3$-3	469.5	–83.8	471.2	–85.5
$3Q^3$-4	465.7	–80.0	467.8	–82.1

NMR measurements provide important information about local Si environments in dumortierite to complement structural information from single-crystal X-ray measurements and chemical information from EMPA. Both Si sites in the dumortierite structure are distinguishable in the ^{29}Si spectrum of D34 and D12, although not in the closely related holtite structure (WPH), where disorder caused by $Ta^{5+} \rightarrow Al^{3+}$ and $(Sb^{3+}, As^{3+}) \rightarrow Si^{4+}$ substitutions broadens the individual signals. Also identifiable in the dumortierite spectrum are multiple smaller peaks, which cross-polarization measurements confirm are adjacent to OH groups and are most likely occurring at the O2 and O7 sites when the Al1 site is vacant. These Q^3 peaks are much smaller in the holtite WPH spectrum, where OH is believed to be less important (Groat et al. 2009; Hoskins et al. 1989).

Acknowledgments

The authors thank M. Pichavant for sample D34, A. Pieczka for sample WPH, the Royal Ontario Museum for sample D12, and R. Friedman for help with the dissolution process. The manuscript was greatly improved by comments from James Kubicki, Jan Cempírek, and two anonymous reviewers, and Associate Editor Brian L. Phillips. Financial support was provided by the Natural Sciences and Engineering Research Council of Canada in the form of Discovery Grants to C.A.F. and L.A.G. The single-crystal and powder X-ray equipment in C-HORSE was purchased with the help of a grant from the Canadian Foundation for Innovation. Electronic structure calculations were performed with computing resources provided by WestGrid and Compute/Calcul Canada.

References cited

Alexander, V.D., Griffen, D.T., and Martin, T.J. (1986) Crystal chemistry of some Fe- and Ti-poor dumortierites. American Mineralogist, 71, 786–794.

Amorós, P., Marcos, M.D., Roca, M., Beltrán-Porter, A., and Beltrán-Porter, D. (1996) Synthetic pathways for new tubular transition metal hydroxy- and fluoro-selenites: crystal structures of $M_{12}(X)_2(SeO_3)_8(OH)_6$ ($M = Co^{2+}$, Ni^{2+}; $X = OH^-$). Journal of Solid State Chemistry, 126, 169–176.

Brunet, F. and Schaller, T. (1996) Protons in the magnesium phosphates phosphoellenbergerite and holtedahlite: An IR and NMR study. American Mineralogist, 81, 385–394.

Casanovas, J., Illas, F., and Pacchioni, G. (2000) Ab initio calculations of ^{29}Si solid state NMR chemical shifts of silane and silanol groups in silica. Chemical Physics Letters, 326, 523–529.

Casserly, T.B. and Gleason, K.K. (2005) Density functional theory calculation of 29Si NMR chemical shifts of organosiloxanes. Journal of Physical Chemistry B, 109, 13605–13610.

Cempírek, J. and Novák, M. (2005) A green dumortierite from Kutná Hora, Moldanubicum, Czech Republic: Spectroscopic and structural study. In F. Pezzotta, Ed., Proceedings of the International Meeting on Crystallization Processes in Granitic Pegmatites, Elba Island (Italy), May 23–28 (http://www.minsocam.org/MSA/Special/Pig/PIG_articles/PIG_articles.html).

Cheeseman, J.R., Trucks, G.W., Keith, T.A., and Frisch, M.J. (1996) A comparison of models for calculating nuclear magnetic resonance shielding tensors. Journal of Chemical Physics, 104, 5497–5509.

Choo, C.O. and Kim, Y. (2003) Textural and spectroscopic studies on hydrothermal dumortierite from an Al-rich clay deposit, southeastern Korea. Mineralogical Magazine, 67, 799–806.

Chopin, C., Ferraris, G., Ivaldi, G., Schertl, H.-P., Schreyer, W., Compagnoni. R., Davidson, C., and Davis, A.M. (1995) Magnesiodumortierite, a new mineral from very-high-pressure rocks (western Alps). II. Crystal chemistry and petrological significance. European Journal of Mineralogy, 7, 525–535.

Clark, T., Chandrasekhar, J., Spitznagel, G.W., and Schleyer, P.v.R. (1983) Efficient diffuse function-augmented basis-sets for anion calculations. 3. The 3-21+G basis set for 1st-row elements, Li-F. Journal of Computational Chemistry, 4, 294–301.

Farges, F., Galoisy, L., Balan, E., Fuchs, Y., and Linarès, J. (2004) Structure and color of the Jack Creek dumortierite (Montana, USA) using spectroscopic approaches. Mitteilungen der Österreichischen Mineralogischen Gesellscahft, 149, 29.

Ferraris, G., Ivaldi, G., and Chopin, C. (1995) Magnesiodumortierite, a new mineral from very-high-pressure rocks (Western Alps). Part I: Crystal structure. European Journal of Mineralogy, 7, 167–174.

Francl, M.M., Pietro, W.J., Hehre, W.J., Binkley, J.S., DeFrees, D.J., Pople, J.A., and Gordon, M.S. (1982) Self-consistent molecular orbital methods. 23. A polarization-type basis set for 2nd-row elements. Journal of Chemical Physics, 77, 3654–3665.

Frisch, M.J., Pople, J.A., and Binkley, J.S. (1984) Self-consistent molecular orbital methods. 25. Supplementary functions for Gaussian basis sets. Journal of Chemical Physics, 80, 3265–3269.

Frisch, M.J., Trucks, G.W., Schlegel, H.B., Scuseria, G.E., Robb, M.A., Cheeseman, J.R., Scalmani, G., Barone, V., Mennucci, B., Petersson, and others. (2009) Gaussian 09, Revision A. 02, Gaussian, Inc., Wallingford, Connecticut.

Fuchs, Y., Ertl, A., Hughes, J.M., Prowatke, S., Brandstaetter, F., and Schuster, R. (2005) Dumortierite from the Gföhl unit: Lower Austria; chemistry, structure, and infra-red spectroscopy. European Journal of Mineralogy, 17, 173–183.

Gardiennet, C., Marcia, F., Fyfe, C.A., and Tekely, P. (2005) Determining the geometry of strongly hydrogen-bonded silanols in a layered hydrous silicate by solid-state nuclear magnetic resonance. Journal of Chemical Physics, 122, 054705.

Golovastikov, N.I. (1965) The crystal structure of dumortierite. Soviet Physics Doklady, 10, 493–495.

Gordon, M.S. (1980) The isomers of silacyclopropane. Chemical Physics Letters, 76, 163–168.

Goreva, J.S., Ma, C., and Rossman, G.R. (2001) Fibrous nanoinclusions in massive rose quartz. The source of rose coloration. American Mineralogist, 86, 466–472.

Grew, E.S. (1996) Borosilicates (exclusive of tourmaline) and boron in rock-forming minerals in metamorphic environments. In E.S. Grew and L.M. Anovitz, Eds., Boron: Mineralogy, Petrology, and Geochemistry, 33, p. 387–502. Reviews in Mineralogy, Mineralogical Society of America, Chantilly, Virginia.

Grew, E.S., Graetsch, H., Pöter, B., Yates, M.G., Buick, I., Bernhardt, H.-J., Schreyer, W., Werding, G., Carson, C.J., Geoffrey L., and Clarke, G.L. (2008) Boralsilite, $Al_{16}B_6Si_2O_{37}$, and "boron-mullite": Compositional variations and associated phases in experiment and nature. American Mineralogist, 93, 283–299.

Groat, L.A., Grew, E.S., Ercit, T.S., and Piezcka, A. (2001) The crystal chemistry of dumortierite and holtite, aluminoborosilicates with heavy elements. Geological Society of America Abstracts with Programs, 33, Abstract 383.

Groat, L.A., Evans, R.J., Grew, E.S., Pieczka, and Ercit, T.S. (2009) The crystal chemistry of holtite. Mineralogical Magazine, 73, 1033–1050.

Hansen, M.R., Jakobsen, H.J., and Skibsted, J. (2003) ^{29}Si Chemical shift anisotropies in calcium silicates from high-field ^{29}Si MAS NMR spectroscopy. Inorganic Chemistry, 42, 2368–2377.

Hoskins, B.F., Mumme, W.G., and Pryce, M.W. (1989) Holtite, $(Si_{2.25}Sb_{0.75})B[(Al_6(Al_{0.43}Ta_{0.27}\square_{0.30})O_{15}(O,OH)_{2.25}]$: crystal structure and crystal chemistry. Mineralogical Magazine, 53, 457–463.

Ikuta, D., Kawame, N., Banno, S., Hirajima, T., Ito, K., Rakovan, J.F., Downs, R.T., and Tamada, O. (2007) First in situ X-ray identification of coesite and retrograde quartz on a glass thin section of an ultrahigh-pressure metamorphic rock and their crystal structure details. American Mineralogist, 92, 57–63.

Kinrade, S.D. and Swaddle, T.W. (1988) Silicon-29 NMR studies of aqueous silicate solutions. 1. Chemical shifts and equilibria. Inorganic Chemistry, 27, 4253–4259.

Klur, I., Jacquinot, J.-F., Brunet, F., Charpentier, T., Virlet, J., Schneider, C., and Tekely, P. (2000) NMR cross-polarization when $T_{1S} > T_{1\rho}$; Examples from silica gel and calcium silicate hydrates. Journal of Physical Chemistry B, 104, 10162–10167.

Kubicki, J.D. and Heaney, P.J. (2003) Molecular orbital modeling of aqueous organosilicon complexes: Implications for silica biomineralization. Geochimica et Cosmochimica Acta, 67, 4113–4121.

Kubicki, J.D. and Toplis, M.J. (2002) Molecular orbital calculations on aluminosilicate tricluster molecules: Implications for the structure of aluminosilicate glasses. American Mineralogist, 87, 668–678.

Ma, C., Goreva, J.S., and Rossman, G.R. (2002) Fibrous nanoinclusions in massive rose quartz: HRTEM and AEM investigations. American Mineralogist, 87, 269–276.

Marcos, M.D., Amorós, P., Beltrán-Porter, A., Martínez-Máñez, R., and Attfield, J.P. (1993) Novel crystalline microporous transition-metal phosphites $M_{11}(HPO_3)_8(OH)_6$ (M = Zn, Co, Ni). X-ray powder diffraction structure determination of the Co and Ni derivatives. Chemistry of Materials, 5, 121–128.

McLean, A.D. and Chandler, G.S. (1980) Contracted Gaussian-basis sets for molecular calculations. 1. 2nd row atoms, Z=11-18. Journal of Chemical Physics, 72, 5639–5648.

Moore, P.B. and Araki, T. (1978) Dumortierite, $Si_3B[Al_{6.75}\square_{0.25}O_{17.25}(OH)_{0.75}]$: a detailed structure analysis. Neues Jahrbuch für Mineralogie, Abhandlungen, 132, 231–241.

Moravetski, V., Hill, J.-R., Eichler, U., Cheetham, A.K., and Sauer, J. (1996) ^{29}Si NMR chemical shifts of silicate species: Ab initio study of environment and structure effects. Journal of the American Chemical Society, 118, 13015–13020.

Pieczka, A. and Marszałek, M. (1996) Holtite—the first occurrence in Poland. Mineralogia Polonica, 27, 3–8.

Pieczka, A., Grew, E.S., Groat, L.A., and Evans, R.J. (2011) Composition of holtite and dumortierite from the Szklary pegmatite, Lower Silesia, Poland. Mineralogical Magazine, 75, 303–315.

Pouchou, J.L. and Pichoir, F. (1985) PAP $\phi(\rho Z)$ procedure for improved quantitative microanalysis. Microbeam Analysis, 1985, 104–106.

Pryce, M.W. (1971) Holtite: a new mineral allied to dumortierite. Mineralogical Magazine, 38, 21–25.

Raade, G., Rømming, C., and Medenbach, O. (1998) Carbonate-substituted phosphoellenbergerite from Modum, Norway: description and crystal structure. Mineralogy and Petrology, 62, 89–101.

Raghavachari, K., Binkley, J.S., Seeger, R., and Pople, J.A. (1980) Self-consistent molecular orbital methods. 20. Basis set for correlated wave-functions. Journal of Chemical Physics, 72, 650–654.

Sindorf, D.W. and Maciel, G.E. (1980) Silicon-29 NMR study of the surface of silica gel by cross-polarization and magic-angle spinning. Journal of the American Chemical Society, 102, 7606–7607.

Smith, J.V. and Blackwell, C.S. (1983) Nuclear magnetic resonance of silica polymorphs. Nature, 303, 223–225.

Smith, K.A., Kirkpatrick, R.J., Oldfield, E., and Henderson, D.M. (1983) High-resolution silicon-29 nuclear magnetic resonance spectroscopic study of rock-forming silicates. American Mineralogist, 68, 1206–1215.

Tossell, J. (2001) Calculating the NMR properties of minerals, glasses and aqueous species. In R.T. Cygan and J.D. Kubicki, Eds., Molecular Modeling Theory and Applications in the Geosciences, 42, p. 437–458. Reviews in Mineralogy and Geochemistry, Mineralogical Society of America, Chantilly, Virginia.

Voloshin, A.V., Gordienko, V.V., Gel'man, Y.M., Zorina, M.L., Yelina, N.A., Kul'chitskaya, Y.A., Men'shikov, Y.P., Polezhayeva, L.I., Ryzhova, R.I., Sokolov, P.B., and Utochkina, G.I. (1977) Holtite (first find in the USSR) and its relationship with other tantalum minerals in rare-metal pegmatites. Novyye Mineraly i Pervyye Nakhodki v SSSR, 106, 337–347 (in Russian).

Werding, G. and Schreyer, W. (1990) Synthetic dumortierite: its PTX-dependent compositional variations in the system Al_2O_3-B_2O_3-SiO_2-H_2O. Contributions to Mineralogy and Petrology, 105, 11–24.

Wolinski, K., Hilton, J.F., and Pulay, P. (1990) Efficient implementation of the Gauge-Independent Atomic Orbital method for NMR chemical shift calculations. Journal of the American Chemical Society, 112, 8251–8260.

Xue, X. and Kanzaki, M. (2000) An ab initio calculation ^{17}O and ^{29}Si NMR parameters for SiO_2 polymorphs. Solid State Nuclear Magnetic Resonance, 16, 245–259.

Manuscript received May 12, 2011
Manuscript accepted November 7, 2011
Manuscript handled by Brian Phillips